A&A 492, 411–417 (2008)
DOI: 10.1051/0004-6361:200810778

Astronomy & Astrophysics

Structure function of the UV variability of Q0957+561

L. J. Goicoechea[1], V. N. Shalyapin[2], R. Gil-Merino[3], and A. Ullán[4]

[1] Departamento de Física Moderna, Universidad de Cantabria, Avda. de Los Castros s/n, 39005 Santander, Spain
e-mail: goicol@unican.es
[2] Institute for Radiophysics and Electronics, National Academy of Sciences of Ukraine, 12 Proskura St., Kharkov 61085, Ukraine
e-mail: vshal@ire.kharkov.ua
[3] Instituto de Física de Cantabria (CSIC-UC), Avda. de Los Castros s/n, 39005 Santander, Spain
e-mail: gilmerino@ifca.unican.es
[4] Robotic Telescopes Group, Centro de Astrobiología (CSIC-INTA), associated to the NASA Astrobiology Institute, Ctra de Ajalvir, km 4, 28850 Torrejón de Ardoz, Madrid, Spain
e-mail: ullanna@inta.es

Received 10 August 2008 / Accepted 24 September 2008

ABSTRACT

We present a detailed structure function analysis of the UV variability of Q0957+561. From optical observations in the 2005−2007 seasons, we constructed normalized structure functions of the quasar luminosity at restframe wavelengths $\lambda \sim 2100$ Å and $\lambda \sim 2600$ Å. Old optical records (1995−1996 seasons) also allow the structure function to be obtained at $\lambda \sim 2100$ Å, but 10 years ago in the observer's frame. These three structure functions are then compared to predictions of both simple and relatively sophisticated (incorporating two independent variable components) Poissonian models. We do not find clear evidence of a chromatic mechanism of variability. From the recent data, ∼100-d time-symmetric and ∼170-d time-asymmetric flares are produced at both restframe wavelengths. Taking into account measurements of time delays and the existence of an EUV/radio jet, reverberation is probably the main mechanism of variability. Thus, two types of EUV/X-ray fluctuations would be generated within or close to the jet and later reprocessed by the disc gas in the two emission rings, at $\lambda \sim 2100$ Å and $\lambda \sim 2600$ Å. The ∼100-d time-symmetric shots are also responsible for most of the ∼2100 Å variability detected in the old experiment (10 years ago). However, there is no evidence of asymmetric shots in the old UV variability. If reverberation is the involved mechanism of variability, this could mean an intermittent production of high-energy asymmetric fluctuations. The old records are also consistent with the presence of very short-lifetime (∼10 d) symmetric flares, which may represent additional evidence of time evolution. Despite these exciting findings, we cannot rule out the possibility of unfortunate gaps in the old light curves (or a relatively short monitoring period) and very short-timescale systematic noise. We also discuss the quasar structure that emerges from the variability scenario.

Key words. gravitational lensing – black hole physics – quasars: general – quasars: individual: Q0957+561

1. Introduction

Structure functions for optical/UV variability of quasars allow investigation of processes that cause intrinsic variations and the properties of intrinsic flares (e.g. Kawaguchi et al. 1998; Cid Fernandes et al. 2000; Vanden Berk et al. 2004; de Vries et al. 2005; Wilhite et al. 2008), the composition of intervening systems (e.g. Lewis & Irwin 1996; Schechter et al. 2003), and the nature of the intergalactic medium (e.g. Hawkins 2002). The most recent and comprehensive study of ensemble structure functions of non-lensed quasars has been presented by Wilhite et al. (2008). In this work, about 2500 quasars at a median redshift of ∼2 were classified into six different groups according to their black hole mass and continuum luminosity. For each group, Wilhite et al. (2008) derived the square root of the noiseless structure function for the *ugriz* bands. They detected the well-known anticorrelation between luminosity and variability, as well as a correlation between variability and black hole mass (see also Wold et al. 2007). Taking these findings into account, most of the variations at restframe time lags ≤1 year are probably intrinsic to the quasars. These might be due to differences in accretion rate. The analysis by Li & Cao (2008) also supports this last claim. However, Wold et al. (2007) and Wilhite et al. (2008) point out the absence of a clear correlation between variability and black hole mass for restframe time lags ≤100 d. Therefore, short timescale variations could not be related to changes in accretion rate.

The Wilhite et al. dataset did not allow for a measurement of the variability of very bright and massive quasars. Moreover, the mechanism of variability might differ from local to distant quasars, and other physical properties (apart from luminosity and black hole mass) may play a role (e.g., circumnuclear activity, presence of a jet, X-ray activity, etc.). Thus, detailed structure functions of well-characterised individual quasars are important tools for understanding different quasar populations. With respect to the individual sources, for example, Cid Fernandes et al. (2000) analysed the members of a sample of optically selected nearby quasars ($z < 0.4$; see Giveon et al. 1999). They used Poissonian models, and derived flare lifetimes and other parameters of interest. A Poissonian model describes physical scenarios in which the luminosity is due to the superposition of a variable component and a constant background (the nonflaring part of the

emissivity). The variable component is made by the superposition of flares, having a given profile and occurring at random times (Cid Fernandes et al. 2000). Cid Fernandes et al. (2000) reported the poor sensitivity of their fits to phenomenological models (flare profiles), with the exception of exponentially decaying flares. These asymmetric flares led to poor fits. Collier & Peterson (2001) also studied optical/UV structure functions of 13 local AGN (Seyfert 1 galaxies) with very good time coverage and resolution. The flare lifetimes (using symmetric triangular flares and certain lag intervals) were $\tau \sim 5-100$ days, with the higher mass AGN having larger variability timescales.

Many previous studies focused on the initial logarithmic slope of the structure function. For example, using the square root of the structure function, a measured initial slope can be compared to predictions of possible physical mechanisms of quasar variability (e.g. Kawaguchi et al. 1998; Hawkins 2002). The initial logarithmic slope β should be less than or equal to 0.5 for square and exponentially decaying flares (Poissonian phenomenological models), whereas symmetric triangular flares produce a steep slope $\beta > 0.5$ (Cid Fernandes et al. 2000; Goicoechea et al. 2008). One can also discuss simple models of the reverberation scenario, i.e., accretion disc flares induced by variable EUV/X-ray irradiation. The cellular-automaton model is able to reproduce a slope $\beta \sim 0.4-0.5$ (Mineshige et al. 1994; Kawaguchi et al. 1998), but cellular-automaton simulations neglect hydrodynamical effects. These might be basic ingredients in the reverberation scenario. The one-dimensional hydrodynamical simulations by Manmoto et al. (1996) led to time-symmetric flares, i.e., flares having symmetric rise and decay. These time-symmetric flares can account for steep growths with slopes above 0.5. The starburst model (supernova explosions) produces an initial slope $\beta \geq 0.7$ (Aretxaga et al. 1997; Kawaguchi et al. 1998), and the microlensing model (extrinsic variability caused by collapsed objects passing close to the sight line toward a quasar) leads to a shallow slope $\beta \sim 0.2-0.3$ (Hawkins 2002). For non-lensed quasars, the slope of the square-root noise-less structure function over restframe lags ≥ 100 d is roughly 0.5 (e.g. Cid Fernandes et al. 2000; Wilhite et al. 2008). On the other hand, local AGN show a variety of initial slopes over restframe lags ≤ 100 d: $\beta \sim 0.3-0.8$ (Collier & Peterson 2001). For timescales $\leq$60 d, Collier & Peterson (2001) also found that optical and UV slopes are consistent with each other. This supports a common variability mechanism.

Over the last 10–15 years, several gravitationally lensed quasars have been monitored more or less regularly. Some of them offer a unique opportunity to study the origin of the intrinsic signal of quasars, since their intrinsic fluctuations are repeated in two or more lensed components with certain time delays and magnitude offsets (e.g. Schneider et al. 1992). Optical frames (g and r bands) of the double quasar Q0957+561 were taken with the Apache Point Observatory (APO) 3.5 m telescope during the 1995 and 1996 seasons. These produced accurate light curves that basically include intrinsic variations (Kundić et al. 1997). Kawaguchi et al. (1998) studied the square root of the structure function of Q0957+561 using the APO g-band light curves (photometric magnitudes), finding a shallow logarithmic slope of ~0.35 over restframe lags $\leq$ 200 d. Unfortunately, these authors did not subtract the observational noise from the photometric measurements (e.g., Simonetti et al. 1985; Cid Fernandes et al. 2000; Collier & Peterson 2001), which has a significant effect on the measured variations at the shortest lags. Gil-Merino et al. (2001) found an initial slope of the square-root noise-less structure function of Q0957+561 in the R band $\beta > 0.5$ (timescale <100 d). Very recently, Fohlmeister et al. (2008) separated intrinsic from extrinsic variations in Q1004+4112, and measured a slope of ~0.5 over restframe lags $\leq$ 1 year (intrinsic structure function in the r band). From r-band data of Q0909+532, Goicoechea et al. (2008) also estimated a steep initial slope $\beta \sim 1$ over restframe lags $\leq$ 100 d. No simple model was able to accurately reproduce the shape of the structure function of the intrinsic luminosity of Q0909+532.

The first lensed quasar Q0957+561 (Walsh et al. 1979) is probably the best-studied lens system. This has been investigated in several spectral regions, including radio, IR, optical, UV and X-ray wavelengths. The radio maps of both components showed the presence of radio cores and ~0.″1 jets (Porcas et al. 1981; Gorenstein et al. 1984, 1988; Garrett et al. 1994; Haarsma et al. 2001). Hutchings (2003) reported evidence for EUV (~1100 Å) activity along the radio jets. Apart from EUV emission associated with the jet, Hutchings (2003) also found EUV emission within a radius of 0.″3, which is associated with a circumnuclear environment. Taking into account the redshift of the quasar ($z = 1.41$), optical observations in the g and r bands correspond to middle ultraviolet (MUV) emission (~2100–2600 Å). Hence, fluctuations in the observed optical magnitude trace variations in the UV luminosity of the source. Q0957+561 is a very bright and massive object, with both λL_λ(1350 Å) and λL_λ(3000 Å) exceeding 10^{46} erg s^{-1}, and a black hole mass of $2-3 \times 10^9\ M_\odot$ (Peng et al. 2006). The double quasar Q0957+561 is also a X-ray bright source (e.g. Chartas 2000), but a possible X-ray jet has not yet been resolved.

Liverpool Quasar Lens Monitoring (LQLM) is a long-term project to follow the variability of gravitationally lensed quasars with the Liverpool robotic telescope (Goicoechea et al. 2008). The first phase of this project (LQLM I) included a monitoring programme of Q0957+561 in the gr optical bands. The new LQLM I light curves of Q0957+561 (2005–2007 seasons) indicated the absence of significant extrinsic variability (Shalyapin et al. 2008). In addition, using the time delays (between quasar components and between optical bands) from the APO and LQLM I records, Shalyapin et al. (2008) suggested that most prominent variations in Q0957+561 are very probably due to reverberation in the accretion disc around the supermassive black hole (see also Collier 2001). In Sect. 2, the new LQLM I dataset is used to accurately trace the shapes of the square-root noise-less structure functions of the quasar UV luminosity. These shapes are closely linked to the nature of the UV fluctuations (see here above), so we investigate the mechanism(s) of variability at two different restframe wavelengths: $\lambda \sim 2100$ Å (g band) and $\lambda \sim 2600$ Å (r band). By comparing the new shape with the old (APO dataset) at $\lambda \sim 2100$ Å, we also check for time evolution of the mechanism(s) of variability. In Sect. 3, we present our conclusions and discuss the quasar structure (temperature profile and source sizes) that emerges from the favoured variability scenario.

2. Structure function analysis

The APO and LQLM I light curves of the double quasar Q0957+561 do not show evidence of extrinsic variability (Kundić et al. 1997; Shalyapin et al. 2008). Thus, we directly obtain the noise-less structure function of the intrinsic luminosity at a given restframe wavelength (instead of one structure function for each component, a combined record and the corresponding structure function are made, e.g., Kawaguchi et al. 1998). The combined records that we use in this paper are depicted in

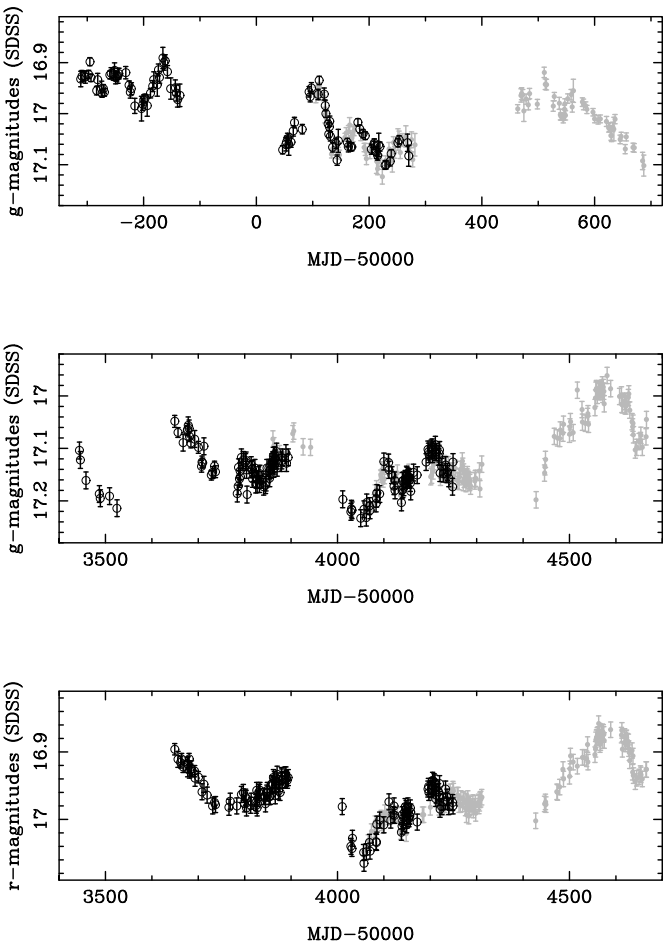

Fig. 1. APO and LQLM I combined light curves. While the light curves of Q0957+561B (open circles) are unchanged, the Q0957+561A records (filled circles) are shifted by the 417-d time delay and optimal magnitude offsets (producing optimal overlaps). *Top*: APO g-band. *Middle*: LQLM I g-band. *Bottom*: LQLM I r-band. We note that all magnitudes are expressed in the SDSS photometric system.

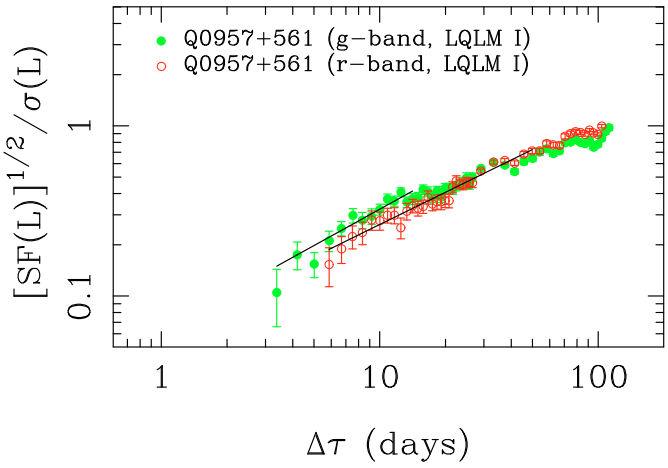

Fig. 2. Normalized structure functions of Q0957+561 from Liverpool telescope (LQLM I) records. These structure functions of the UV luminosities at ∼2100 Å (g band; filled circles) and ∼2600 Å (r band; open circles) are accurately described from very short restframe lags (∼1−10 days) to lags when $[SF(L)]^{1/2}/\sigma(L) \sim 1$ (asymptotic behaviours). The initial growths are consistent with slopes $\beta \sim 0.6$−0.8 (solid lines).

Fig. 1. There is no standard form of the structure function, but different approaches to the problem. For example, while magnitudes, $SF(m)$, are often used in optical astronomy (e.g. Wilhite et al. 2008, and references therein), monochromatic fluxes or luminosities, $SF(F)$ or $SF(L)$, are more relevant in radio astronomy or to accurately compare with models of variability (e.g. Simonetti et al. 1985; Cid Fernandes et al. 2000; Collier & Peterson 2001). The structure function $SF(L)$ at restframe lag $\Delta\tau$ is estimated through the averaged sum

$$SF(L) = (1/2N) \sum_{i,j} [(10^{-0.4m_j} - 10^{-0.4m_i})^2 - \overline{\sigma}_i^2 - \overline{\sigma}_j^2], \qquad (1)$$

where m are magnitudes, $\overline{\sigma} = 0.921 \times 10^{-0.4m}\sigma$, σ are photometric uncertainties, and the sum includes N pairs verifying $\tau_j - \tau_i \sim \Delta\tau$. Here, $L = 10^{-0.4m}$ are monochromatic luminosities in convenient units and τ are restframe times (e.g., Cid Fernandes et al. 2000; Goicoechea et al. 2008). This $SF(L)$ describes typical luminosity variabilities at different restframe lags. We normalize the original structure function to the luminosity variance and then take the square-root for convenience, i.e., we analyse the normalized structure function $f = [SF(L)]^{1/2}/\sigma(L)$.

Restframe lags substantially below the restframe duration of the records are considered in the analysis. In the initial selection, we take $\Delta\tau \leq P/4(1+z)$, where P is the duration of each whole combined record (see Fig. 1). Later, only lags before reaching the asymptotic behaviours ($f \leq 1$) are taken into account. In Fig. 2, using LQLM I observations, the normalized structure function at $\lambda \sim 2100$ Å (g band; filled circles) is compared to f at $\lambda \sim 2600$ Å (r band; open circles). Both growths seem to be consistent with each other. With respect to the initial logarithmic slopes, in Fig. 2 we also show two fits $f = A(\Delta\tau)^{\beta}$ with $\hat{\chi}^2 = \chi^2/N_{\rm d.o.f.}$ values close to 1 ($N_{\rm d.o.f.}$ is the number of degrees of freedom). The fits over time intervals 3−14 d (g band) and 6−50 d (r band) lead to $\beta = 0.71 \pm 0.08$ and $\beta = 0.63 \pm 0.02$ (1σ intervals), respectively. These initial slopes disagree with the prediction of the cellular-automaton disc-instability model, but roughly agree with the time-symmetric flares that appear in the one-dimensional hydrodynamical simulations (see Introduction). In principle, the starburst model could also account for the measured slope at ∼2100 Å (g band). The microlensing slope $\beta \sim 0.2$−0.3 (Hawkins 2002) is strongly inconsistent with the LQLM I data of Q0957+561, which is not at all surprising. We are studying intrinsic fluctuations, so microlensing does not play any role.

In Fig. 3, the APO (open triangles) and LQLM I (filled circles) structure functions of Q0957+561 at ∼2100 Å have significantly different initial growths. This may be a consequence of evolution in the variability scenario, since both experiments (APO and LQLM I) are separated by ∼1500 d in the quasar restframe. In fact, the oldest (APO) brightness records seem to incorporate relatively short fluctuations (which would not be present in the LQLM I light curves) that would generate the differences between initial growths. The solid lines in Fig. 3 fit the APO behaviours in three time intervals ($\hat{\chi}^2 \sim 1$). Their slopes are $\beta = 0.81 \pm 0.12$ at $\Delta\tau \leq 5$ d, $\beta = 0.66 \pm 0.06$ at $\Delta\tau \leq 11$ d, and $\beta = 0.59 \pm 0.04$ at $\Delta\tau \leq 16$ d (1σ intervals).

In order to discuss the mechanism(s) for (M)UV variability, and to quantify the spectral and time evolution of that mechanism(s), we compare the observed shapes of the structure functions (Figs. 2−3) with predictions of Poissonian models. In a first level of complexity (simplest models), we use three phenomenological models: square flares (SQF), exponentially

Table 1. Solutions for the main Poissonian models.

Model[a]	Observed structure function[b]	$\hat{\chi}^2$	w_1[c]	τ_1[c] (d)	τ_2[c] (d)
SQF(1)+STF(2)	$f_{\rm LQLM\ I}$(2100 Å)	1.21	$0.266^{+0.016}_{-0.020}$	$32.6^{+1.4}_{-2.4}$	$175.8^{+7.2}_{-6.6}$
	$f_{\rm LQLM\ I}$(2600 Å)	0.65	$0.170^{+0.028}_{-0.016}$	$33.2^{+4.2}_{-1.6}$	$122.7^{+4.2}_{-3.9}$
	$f_{\rm APO}$(2100 Å)	1.44	$0.266^{+0.024}_{-0.024}$	$11.0^{+1.4}_{-1.2}$	$107.1^{+6.6}_{-6.0}$
SQF(1)+SBF(2)	$f_{\rm LQLM\ I}$(2100 Å)	1.19	$0.706^{+0.092}_{-0.664}$	$151.4^{+10.8}_{-142.2}$	135^{+161}_{-29}
	$f_{\rm LQLM\ I}$(2600 Å)	0.99	$0.630^{+0.080}_{-0.082}$	$88.2^{+4.0}_{-6.0}$	353^{+108}_{-52}
	$f_{\rm APO}$(2100 Å)	1.78	$0.758^{+0.042}_{-0.046}$	$99.4^{+8.6}_{-6.8}$	32^{+6}_{-6}
EDF(1)+STF(2)	$f_{\rm LQLM\ I}$(2100 Å)	1.25	$0.902^{+0.042}_{-0.268}$	$180.4^{+14.0}_{-62.8}$	$90.6^{+107.7}_{-26.1}$
	$f_{\rm LQLM\ I}$(2600 Å)	0.73	$0.418^{+0.048}_{-0.054}$	$154.8^{+27.6}_{-30.4}$	$97.2^{+9.6}_{-7.2}$
	$f_{\rm APO}$(2100 Å)	1.80	$0.856^{+0.032}_{-0.030}$	$135.6^{+14.0}_{-12.4}$	$10.8^{+1.5}_{-1.5}$
STF(1)+STF(2)	$f_{\rm LQLM\ I}$(2100 Å)	1.55	$0.204^{+0.020}_{-0.018}$	$24.3^{+2.4}_{-2.7}$	$162.3^{+6.3}_{-5.7}$
	$f_{\rm LQLM\ I}$(2600 Å)	0.80	$0.182^{+0.046}_{-0.036}$	$36.0^{+5.4}_{-5.1}$	$123.9^{+5.7}_{-5.1}$
	$f_{\rm APO}$(2100 Å)	1.31	$0.270^{+0.018}_{-0.020}$	$10.8^{+0.9}_{-0.9}$	$108.0^{+6.3}_{-5.7}$
STF(1)+SBF(2)	$f_{\rm LQLM\ I}$(2100 Å)	1.18	$0.052^{+0.586}_{-0.010}$	$11.7^{+177.3}_{-2.1}$	287^{+13}_{-192}
	$f_{\rm LQLM\ I}$(2600 Å)	0.72	$0.608^{+0.110}_{-0.098}$	$112.5^{+6.0}_{-8.4}$	167^{+35}_{-40}
	$f_{\rm APO}$(2100 Å)	1.64	$0.646^{+0.036}_{-0.036}$	$114.3^{+8.4}_{-7.8}$	33^{+5}_{-4}

[a] SQF = square flares, EDF = exponentially decaying flares, STF = symmetric triangular flares, and SBF = starburst flares.
[b] Normalized structure functions (see main text) from Liverpool telescope (LQLM I) and Apache Point Observatory (APO) data.
[c] All measurements are 1σ intervals.

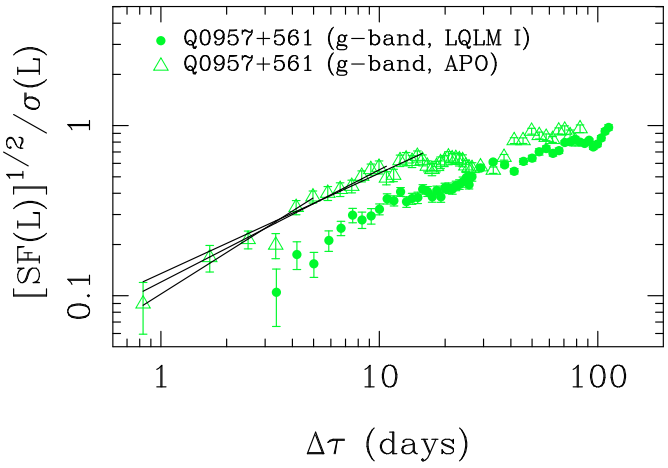

Fig. 3. Normalized structure functions of Q0957+561 from Apache Point Observatory (APO) and Liverpool telescope (LQLM I) records. The two structure functions of the luminosity at ∼2100 Å (APO = open triangles, LQLM I = filled circles) correspond to two experiments separated by ∼10 years, i.e., ∼4 years in the quasar restframe. The initial logarithmic slopes (see solid lines) of the APO trend vary from $\beta \sim 0.8$ over lags ≤ 5 d to $\beta \sim 0.6$ over lags ≤ 16 d.

decaying flares (EDF), and symmetric triangular flares (STF), as well as starburst flares (SBF) produced by supernova explosions (Aretxaga et al. 1997; Cid Fernandes et al. 2000). For example, EDF is a simple model to describe asymmetric flares, i.e., rapid rises and slow declines, or slow rises and rapid declines (the structure function cannot distinguish between both variants). STF is a rough description of the hydrodynamical simulations by Manmoto et al. (1996) and a relatively good approach to the X-ray shots found by Negoro et al. (1994). Each model is characterised by a shape function $s(\tau)$, $f = [s(\tau)]^{1/2}$, and these shape functions appear in Appendix B of Cid Fernandes et al. (2000) and Eq. (17) of Aretxaga et al. (1997). The 4 level-1 models of f only include one free parameter: flare lifetime τ (e.g., $\tau = T$ for a square flare of duration T and $\tau = 5\,t_{sg}$ for a supernova explosion, where t_{sg} is the time when the supernova remnant reaches the maximum of its radiative phase). In the Poissonian framework, we can consider more complex schemes. Thus, in a second level of complexity, the luminosity is assumed to be due to the superposition of a constant background and two independent variable components. It can easily be shown that $f = [w_1 s_1(\tau_1) + (1-w_1) s_2(\tau_2)]^{1/2}$, where w_1 is the ratio between the variance of the first fluctuating component and the total variance, and s_1 and s_2 are the shape functions of the two independent components.

The possibility that AGN variability is caused by several independent processes was suggested in previous work (e.g. Kawaguchi et al. 1998; Collier & Peterson 2001). Here, using 10 level-2 models of f (SQF+SQF, SQF+EDF, SQF+STF, SQF+SBF, EDF+EDF, EDF+STF, EDF+SBF, STF+STF, STF+SBF, and SBF+SBF), we also explore this possibility. Each of these 10 possible combinations is characterised by three free parameters: w_1, and two lifetimes τ_1 and τ_2 (see above). To evaluate the quality of the fits obtained with the full set of 14 models, we analyse the $\hat{\chi}^2$ (reduced chi-square) values. For an acceptable fit, χ^2 is expected to be in the range $N_{\rm d.o.f.} \pm 2(2N_{\rm d.o.f.})^{1/2}$ (allowing $\chi^2 - N_{\rm d.o.f.}$ differences of up to two standard deviations of the χ^2 distribution), which implies $0.6 \leq \hat{\chi}^2 \leq 1.4$ ($N_{\rm d.o.f.} \sim 45$). As expected from the measured slopes, the five best solutions in terms of $\hat{\chi}^2$ are associated with (level-2) models incorporating either STF, or SBF, or both of them. However, only one out of our 42 fits to $f_{\rm LQLM\ I}$(2100 Å), $f_{\rm LQLM\ I}$(2600 Å), and $f_{\rm APO}$(2100 Å) (3 observed shapes ×14 models) gives $\hat{\chi}^2 \leq 1.4$. This result means that the uncertainties are slightly underestimated or alternatively, the models do not describe all details. The statistical uncertainties in each structure function, see Eq. (1), are computed as the standard deviations of the means (averaged sums) for the different time lag bins. Although we use a very popular estimator of uncertainties, Collier & Peterson (2001) noted that not all pairs of data in a given bin are independent. To address this problem, they multiplied their errors by $2^{1/2}$. We adopt the Collier & Peterson's perspective and fit again the observed structure functions.

After slightly enlarging the error bars, we concentrate on level-2 models consisting of STF/SBF and anything else. Among

these 7 models of f, we select those giving $\hat{\chi}^2 < 2$ for the three observed structure functions (main Poissonian models). The set of solutions is presented in Table 1. With regard to the spectral behaviour, four out of the 5 models in Table 1 are able to accurately and simultaneously describe $f_{\rm LQLM\ I}(2100\ \text{Å})$ and $f_{\rm LQLM\ I}(2600\ \text{Å})$, i.e., they fit both LQLM I shapes acceptably well ($0.6 \leq \hat{\chi}^2 \leq 1.4$). The solutions for the first model (SQF+STF) indicate that symmetric triangular flares at ~2100 Å have a lifetime longer than the duration of STF at ~2600 Å. However, this is puzzling with the accretion disc paradigm. Similar lifetimes are expected in a reverberation scenario. Moreover, $\tau(2100\ \text{Å}) < \tau(2600\ \text{Å})$ in a disc local-instability scenario, e.g., the thermal timescale is proportional to $(R^3/GM)^{1/2}$, where M is the mass of the central black hole and $R \propto \lambda^{4/3}$ is the emission radius (e.g., Goicoechea et al. 2008, and references therein). The solutions for the second model (SQF+SBF) incorporate supernova explosions with $t_{sg}(2100\ \text{Å}) < t_{sg}(2600\ \text{Å})$. However, the timescale t_{sg} is exlusively related to the circumstellar density and the total energy released in each explosion (e.g., Aretxaga et al. 1997), so a chromatic timescale is not the expected result.

The solutions for the EDF+STF and STF+SBF models are the most interesting ones (LQLM I data). There is a clear degeneracy between EDF and SBF, which seem to work in a similar way. Hence, the solutions for the third and fifth models are interpreted as evidence in favour of the coexistence of ~100-d time-symmetric flares and longer time-asymmetric shots (see Table 1). Both kinds of flares at both wavelengths can be mostly due to reverberation, i.e., two types of EUV/X-ray variation in the vicinity of the accretion disc axis that are reprocessed by two annuli of the disc gas. Measurements of time delays (Kundić et al. 1997; Collier 2001; Shalyapin et al. 2008), and the existence of an EUV jet (Hutchings 2003) and a bright X-ray source (Chartas 2000), support this physical scenario. From Table 1, $\tau_{\rm asym} = 168$ d and $\tau_{\rm sym} = 105$ d is a good compromise between the results at the two wavelengths and for the two flare asymmetric profiles (exponentially decaying and starburst profile). Although the relative variances depend on wavelength, there is no need to invoke some mechanism other than reverberation. While the ~2100 Å variability is consistent with the asymmetric flares producing most of the variance at this wavelength ($w_{\rm asym} = 72\%$), the variance at ~2600 Å would be mainly due to the symmetric flares ($w_{\rm asym} = 40\%$). This chromaticity in the relative variances is associated with the difference between time coverages, gaps and artifacts in the g (~2100 Å) and r (~2600 Å) bands (see middle and bottom panels in Fig. 1). The LQLM I g-band combined record lasts longer than the LQLM I combined curve in the r band, so it contains a prominent decline that is not present in the shorter record. Besides the longer time coverage, the g-band curve fills a gap corresponding to the peak of an important event. The presence of a few artifacts could also play a role. In Fig. 4, the LQLM I shapes are compared with the adopted solutions: $w_{\rm asym} = 0.72$, $\tau_{\rm asym} = 168$ d, and $\tau_{\rm sym} = 105$ d for $f_{\rm LQLM\ I}(2100\ \text{Å})$, and $w_{\rm asym} = 0.40$, $\tau_{\rm asym} = 168$ d, and $\tau_{\rm sym} = 105$ d for $f_{\rm LQLM\ I}(2600\ \text{Å})$.

In spite of the enlargement of error bars and the use of relatively sophisticated modelling, no model leads to an acceptable global solution at both wavelengths and both epochs. The APO data are only consistent, in terms of $\hat{\chi}^2$, with the STF+STF model. The corresponding solution includes ~100-d time-symmetric flares and other family of very short-lifetime ($\tau \sim 10$ d) symmetric flares. This last kind of fluctuations is responsible for about 1/4 of the total variance. The dominant ~100-d shots are also detected in the LQLM I experiment, so the main source of these flares do not evolve over decades (in the observer's frame). Nevertheless, the absence of longer asymmetric flares (APO data) is a mystery. This could be due to unfortunate gaps in the light curves, time coverage of the monitoring, etc, or simply reflects the evolution of the central engine. Assuming that UV asymmetric flares are triggered by EUV/X-ray fluctuations (reverberation in the accretion disc; see above), we would be dealing with intermittency in the generation of high-energy asymmetric fluctuations (within or close to the jet). As we commented here above, the structure function $f_{\rm APO}(2100\ \text{Å})$ agrees with the presence of very short-timescale shots, which are not detected from the new LQLM I records. These fluctuations may be caused by some kind of observational (systematic) noise or alternatively, they might be related to an episode of very short-timescale activity inside the disc, the jet or other region. In Fig. 4, the adopted solution (STF+STF model with parameters $w_1 = 0.27$, $\tau_1 = 11$ d, and $\tau_2 = 105$ d) fits $f_{\rm APO}(2100\ \text{Å})$ reasonably well.

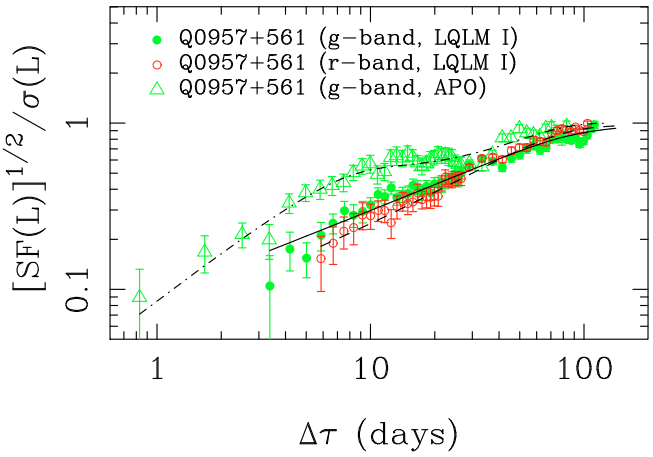

Fig. 4. Observed structure functions and adopted solutions. For the LQLM I experiment, we show EDF+STF laws with parameters: $w_1 = 0.72$, $\tau_1 = 168$ d, and $\tau_2 = 105$ d (g band; solid line), and $w_1 = 0.40$, $\tau_1 = 168$ d, and $\tau_2 = 105$ d (r band; dashed line). SBF+STF laws with the above parameters are also able to reproduce the LQLM I shapes. For the APO data in the g band, we display a STF+STF law with parameters: $w_1 = 0.27$, $\tau_1 = 11$ d, and $\tau_2 = 105$ d (dashed-dotted line).

3. Conclusions and discussion

We present a novel and rigorous analysis of the structure function of the UV variability of the gravitationally lensed quasar Q0957+561. New Liverpool telescope data (2005−2007 seasons; Shalyapin et al. 2008) allow us to construct normalized structure functions of the quasar luminosity at two restframe wavelengths: $\lambda \sim 2100$ Å (g band data) and $\lambda \sim 2600$ Å (r band data). Old Apache Point Observatory records in the g band (1995−1996 seasons; Kundić et al. 1997) are also used to check the possible time evolution of the variability at ~2100 Å. The observed shapes of the structure functions are compared to predictions of a large set of Poissonian models. This set of models includes the simplest and well-known ones, consisting of only one variable component (Cid Fernandes et al. 2000, and references therein), as well as hybrid models incorporating two independent variable components.

Several hybrid (or level-2) models are able to account for both Liverpool telescope structure functions (see Table 1). Some of them contain flares with unrealistic profile (square flares) and lead to solutions that are difficult to interpret. Fortunately, we also find reasonable solutions in which ∼100-d time-symmetric and ∼170-d time-asymmetric flares are produced at both restframe wavelengths. Exponentially decaying and starburst flares (and very probably other time-asymmetric shots) work in a similar way. Therefore, the good behaviour of the starburst ingredient does not necessarily implies the existence of supernova explosions, but the production of highly asymmetric shots. What about the mechanism of intrinsic variability?. The old and very recent *gr* light curves of Q0957+561 led to time delays between quasar components and between optical bands that mainly support a reverberation scenario (Collier 2001; Shalyapin et al. 2008). Thus, reverberation would be the main mechanism of variability. The presence of an EUV/radio jet (e.g., Garrett et al. 1994; Hutchings 2003) and a bright X-ray source (Chartas 2000) also suggests the viability of this mechanism: two types of EUV/X-ray fluctuations that are generated within or close to the jet, and later reprocessed by two rings of the disc (each ring corresponds to a different restframe wavelength). On the other hand, one can also justify both kinds of flare profile. For example, the cellular-automaton model produces asymmetric shots (e.g., Kawaguchi et al. 1998), and hydrodynamical simulations lead to symmetric flares (Manmoto et al. 1996).

The ∼100-d time-symmetric shots seem to be also responsible for most of the ∼2100 Å variability detected in the Apache Point Observatory experiment, but there is no evidence of asymmetric shots in the old UV variability. This absence of asymmetric flares may be due to gaps in the light curves, a relatively short monitoring period, etc. Alternatively, it could means an evolution of the central engine, i.e., intermittent production of high-energy asymmetric fluctuations. The Apache Point Observatory structure function is also consistent with the presence of very short-lifetime (∼10 d) symmetric flares. This kind of flare might be caused by observational systematic noise, or perhaps, represent additional evidence for time evolution. Our results do not support a previous claim for the possible starburst origin of some events in the old *g*-band light curves (Ullán et al. 2003). Despite the presence of two twin events (one in each quasar component) with an anomalous delay (Goicoechea 2002), the associated shot probably occurred at the base of the jet or in the circumnuclear region, but it was not originated by a supernova explosion.

Very recently, several studies have showed evidence that optical/UV variability of quasars on restframe timescales >100 d is mainly driven by variations in accretion rate (e.g., Wold et al. 2007; Arévalo et al. 2008; Li & Cao 2008; Wilhite et al. 2008). Here we are discussing the UV variability of Q0957+561 at restframe lags ≤100 d. Q0957+561 is a very bright and massive object, and this population could not be studied by Wilhite et al. (2008). The first lensed quasar has also an EUV/radio jet (and important X-ray activity; see above), so high-energy variations in the surroundings of the disc axis and their reverberation are possible. For example, on timescales below 100 days, the optical variations of the local Seyfert galaxy NGC 5548 are related to its X-ray variations (Czerny et al. 1999). Hence, part of the optical variability of this AGN (timescales <100 days) could be explained by X-ray reprocessing. Chromatic delays for the local Seyfert galaxy NGC 7469 also reveal a reverberation scenario (Collier et al. 1999). Arévalo et al. (2008) reported on an illustrative example of mixed variability. The local quasar MR 2251-178 has been monitored simultaneously in X-rays and optical bands. All spectral regions were significantly variable, and the fluctuations were clearly correlated. Arévalo et al. (2008) indicated that pure reprocessing of X-rays cannot account for both ∼100-d and ∼500-d timescale optical variability. They claimed that two distinct mechanisms produce the variability: accretion rate variations plus reverberation, and the shortest timescale optical events are due to reverberation.

For an irradiated disc, in general, we obtain a temperature profile shallower than the standard one $T \propto r^{-3/4}$ (Shakura & Sunyaev 1973). The reverberation hypothesis assumes that the optical/UV disc regions are irradiated by EUV/X-ray photons from the vicinity of the disc axis. If the high-energy source is placed on the axis and at a height H_X above the thin disc (disc thickness $\ll H_X$), the non-standard temperature profile is

$$T(r) = \left[\frac{3GM\dot{M}}{8\pi\sigma r^3} + \frac{(1-A)L_X H_X}{4\pi\sigma(H_x^2 + r^2)^{3/2}}\right]^{1/4}, \quad (2)$$

where G is the gravitation constant, σ is the Stefan constant, $\dot{M}$ is the mass accretion rate, A is the disc albedo, i.e., the ratio of reflection to incident high-energy radiation, and L_X is the luminosity of the irradiating source (e.g., Cackett et al. 2007, and references therein). Moreover, considering $r \gg H_X$ (and thus, a standard temperature profile), the typical radius of the intensity distribution at a given restframe wavelength λ should be greater than the standard value (for standard structure, see, e.g., Shalyapin et al. 2002). Equation (2) leads to

$$R = \left[\frac{3GM\dot{M}}{8\pi\sigma} + \frac{(1-A)L_X H_X}{4\pi\sigma}\right]^{1/3}\left[\frac{k\lambda}{hc}\right]^{4/3}, \quad (3)$$

where k is the Boltzmann constant, h is the Planck constant, and c is the speed of light. This non-standard typical radius is produced by both the heating due to irradiation and the viscous heating in the disc. Finally, we point out that shallow temperature profiles (from reverberation) could be consistent with microlensing data of some lensed quasars (e.g., Poindexter et al. 2008). Moreover, the non-standard sizes of several lensed and microlensed quasars (Morgan et al. 2007; Pooley et al. 2007) might be related to relatively high irradiation-to-viscosity ratios $IVR = 2(1-A)L_X H_X/3GM\dot{M}$.

Acknowledgements. We thank an anonymous referee for several comments that improved the presentation of our results. Liverpool Quasar Lens Monitoring is a long-term project to follow the optical variability of lensed quasars with the Liverpool robotic telescope. This paper is partially based on the results of the first phase of this project (LQLM I; see the Web site http://grupos.unican.es/glendama/index.htm). We acknowledge the continuing support of the Liverpool telescope team. We also thank T. Kundić and other members of the APO collaboration for providing light curves to us. This research has been supported by the Spanish Department of Education and Science grant AYA2007-67342-C03-02 and University of Cantabria funds. R.G.M. holds a grant of the ESP2006-13608-C02-01 project financed by the Spanish Department of Science and Innovation.

References

Aretxaga, I., Cid Fernandes, R., & Terlevich, R. 1997, MNRAS, 286, 271
Arévalo, P., Uttley, P., Kaspi, S. et al. 2008, MNRAS, 389, 1479
Cackett, E. M., Horne, K., & Winkler, H. 2007, MNRAS, 380, 669
Chartas, G. 2000, ApJ, 531, 81
Cid Fernandes, R., Sodré, Jr. L., & Vieira da Silva, Jr. L. 2000, ApJ, 544, 123
Collier, S. 2001, MNRAS, 325, 1527
Collier, S., & Peterson, B. M. 2001, ApJ, 555, 775
Collier, S., Horne, K., Wanders, I., & Peterson, B. M. 1999, MNRAS, 302, L24
Czerny, B., Schwarzenberg-Czerny, A., & Loska, Z. 1999, MNRAS, 303, 148

de Vries, W. H., Becker, R. H., White, R. L., & Loomis, C. 2005, AJ, 129, 615
Fohlmeister, J., Kochanek, C. S., Falco, E. E., Morgan, C. W., & Wambsganss, J. 2008, ApJ, 676, 761
Garrett, M. A., Calder, R. J., Porcas, R. W., et al. 1994, MNRAS, 270, 457
Gil-Merino, R., Goicoechea, L. J., Serra-Ricart, M., et al. 2001, MNRAS, 322, 397
Giveon, U., Maoz, D., Kaspi, S., Netzer, H., & Smith, P. S. 1999, MNRAS, 306, 637
Goicoechea, L. J. 2002, MNRAS, 334, 905
Goicoechea, L. J., Shalyapin, V. N., Koptelova, E., et al. 2008, New A, 13, 182
Gorenstein, M. V., Shapiro, I. I., Rogers, A. E. E., et al. 1984, ApJ, 287, 538
Gorenstein, M. V., Cohen, N. L., Shapiro, I. I., et al. 1988, ApJ, 334, 42
Haarsma, D., Lehár, J., & Barkana, R. 2001, ASP Conf. Proc., 237, 89
Hawkins, M. R. S. 2002, MNRAS, 329, 76
Hutchings, J. B. 2003, AJ, 126, 24
Kawaguchi, T., Mineshige, S., Umemura, M., & Turner, E. L. 1998, ApJ, 504, 671
Kundić, T., Turner, E. L., Colley, W. N., et al. 1997, ApJ, 482, 75
Lewis, G. F., & Irwin, M. J. 1996, MNRAS, 283, 225
Li, S.-L., & Cao, X. 2008, MNRAS, 387, L41
Manmoto, T., Takeuchi, M., Mineshige, S., Matsumoto, R., & Negoro, H. 1996, ApJ, 464, L135
Mineshige, S., Ouchi, B. N., & Nishimori, H. 1994, PASJ, 46, 97
Morgan, C. W., Kochanek, C. S., Morgan, N. D., & Falco, E. E. 2007, ApJ, submitted [arXiv:0707.0305]
Negoro, H., Miyamoto, S., & Kitamoto, S. 1994, ApJ, 423, L127
Peng, C. Y., Impey, C. D., Rix, H.-W., et al. 2006, ApJ, 649, 616
Poindexter, S., Morgan, N., & Kochanek, C. S. 2008, ApJ, 673, 34
Pooley, D., Blackburne, J. A., Rappaport, S., & Schechter, P. L. 2007, ApJ, 661, 19
Porcas, R. W., Booth, R. S., Browne, I. W. A., Walsh, D., & Wilkinson, P. N. 1981, Nature, 289, 758
Schechter, P. L., Udalski, A., Szymański, M., et al. 2003, ApJ, 584, 657
Schneider, P., Ehlers, J., & Falco, E. E. 1992, Gravitational Lenses (Berlin: Springer)
Shakura, N. I., & Sunyaev, R. A. 1973, A&A, 24, 337
Shalyapin, V. N., Goicoechea, L. J., Alcalde, D., et al. 2002, ApJ, 579, 127
Shalyapin, V. N., Goicoechea, L. J., Koptelova, E., Ullán, A., & Gil-Merino, R. 2008, A&A, 492, 401
Simonetti, J. H., Cordes, J. M., & Heeschen, D. S. 1985, ApJ, 296, 46
Ullán, A., Goicoechea, L. J., Munōz, J. A., et al. 2003, MNRAS, 346, 415
Vanden Berk, D. E., Wilhite, B. C., Kron, R. G., et al. 2004, ApJ, 601, 692
Walsh, D., Carswell, R. F., & Weymann, R. J. 1979, Nature, 279, 381
Wilhite, B. C., Brunner, R. J., Grier, C. J., Schneider, D. P., & Vanden Berk, D. E. 2008, MNRAS, 383, 1232
Wold, M., Brotherton, M. S., & Shang, Z. 2007, MNRAS, 375, 989